LETTERS

Enhanced current transport at grain boundaries in high-T_c superconductors

R. F. Klie[1], J. P. Buban[2], M. Varela[3], A. Franceschetti[3,4], C. Jooss[5], Y. Zhu[1], N. D. Browning[6], S. T. Pantelides[3,4] & S. J. Pennycook[3,4]

Large-scale applications of high-transition-temperature (high-T_c) superconductors, such as their use in superconducting cables, are impeded by the fact that polycrystalline materials (the only practical option) support significantly lower current densities than single crystals[1–6]. The superconducting critical current density (J_c) across a grain boundary drops exponentially if the misorientation angle exceeds 2°–7°. Grain texturing reduces the average misorientation angle, but problems persist[7,8]. Adding impurities (such as Ca in $YBa_2Cu_3O_{7-\delta}$; YBCO) leads to increased J_c (refs 9, 10), which is generally attributed to excess holes introduced by Ca^{2+} substituting for Y^{3+} (ref. 11). However, a comprehensive physical model for the role of grain boundaries and Ca doping has remained elusive. Here we report calculations, imaging and spectroscopy at the atomic scale that demonstrate that in poly-crystalline YBCO, highly strained grain-boundary regions contain excess O vacancies, which reduce the local hole concentration. The Ca impurities indeed substitute for Y, but in grain-boundary regions under compression and tension they also replace Ba and Cu, relieving strain and suppressing O-vacancy formation. Our results demonstrate that the ionic radii are more important than their electronic valences for enhancing J_c.

The enhancement of grain-boundary J_c in poly-crystalline YBCO has now been widely reported, induced by Ca doping of both weak-linked high-angle[9,10], and strongly-coupled low-angle, grain boundaries[12,13]. However, Ca doping has been shown to reduce T_c. The ideal dopant, which has yet to be found, would improve the grain-boundary J_c, but not adversely affect other superconducting properties, such as the T_c of the grains. It is usually assumed that the doping mechanism is electronic in nature, resulting in reduction of the intrinsic grain-boundary charge[9,10,14], modification of the bulk screening length[9,10] or reduction of both charge and strain fields[13,15]. However, a comprehensive atomic-scale model has not yet been found that can explain the impact of grain boundaries and Ca impurities on the critical current density. Single-crystal studies show that Ca^{2+} substitutes for Y^{3+} where it acts as a hole dopant[11]. Song *et al.* (personal communication, and ref. 16) have found that Ca segregates in grain boundaries, and it was generally believed that Ca replaces Y there as well. However, strains of more than 10% can occur at the dislocation cores that comprise grain boundaries, with severe consequences. For example, $SrTiO_3$ grain boundaries are intrinsically non-stoichiometric owing to such high strains[17,18]. Similar effects are expected in YBCO.

The formation energies required for substituting an isolated Ca dopant on different lattice sites in YBCO (in an oxidizing environment) as a function of biaxial strain in the *a*–*b* plane were calculated from first principles, and are shown in Fig. 1a. In unstrained YBCO, Ca substitutes for Y as expected[19]. In regions under compressive strain, however, substitution for Ba is increasingly possible and becomes energetically favourable at strains greater than ~6%. Similarly, in regions under tensile strain, substitution for Cu becomes favourable. In contrast, strain has only a small effect on substitution for Y. Clearly, the relative ionic sizes drive the defect formation

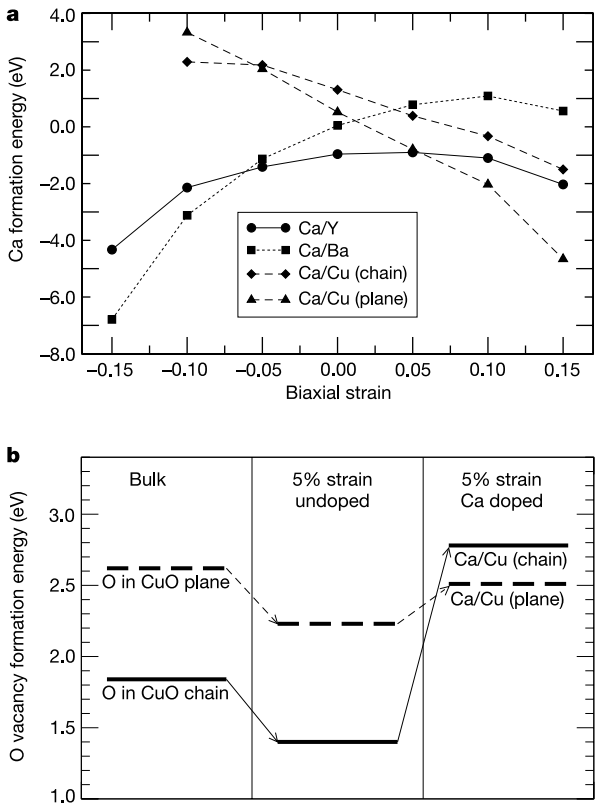

Figure 1 | First-principles calculations of Ca and O vacancy formation energy in bulk YBCO. a, Energy required to substitute Ca on different lattice sites in YBCO as a function of biaxial strain. It can be energetically favourable for Ca to replace Y, Ba or Cu, depending on the local strain. **b**, Formation energy of O vacancies in bulk YBCO (left panel), in undoped YBCO under 5% tensile strain in the *a*–*b* plane (central panel), and in Ca-doped YBCO under 5% tensile strain (right panel), simulating the expanded regions at grain boundaries. For doped grain boundaries where Ca substitutes Cu, the O vacancy formation energy increases significantly.

[1]Center for Functional Nanomaterials, Brookhaven National Laboratory, Upton, New York 11973, USA. [2]Institute of Engineering Innovation, The University of Tokyo, Tokyo, 113-8656, Japan. [3]Condensed Matter Sciences Division, Oak Ridge National Laboratory, Oak Ridge, Tennessee 37831, USA. [4]Department of Physics and Astronomy, Vanderbilt University, Nashville, Tennessee 37235, USA. [5]Institut für Materialphysik, University of Göttingen, 37073 Göttingen, Germany. [6]Department of Chemical Engineering and Materials Science, University of California-Davis, Davis, California 95616, USA.

© 2005 Nature Publishing Group

energies: the ionic radii of Ca and Y are roughly equal, but the radius of Cu is ~30% smaller and the radius of Ba is ~30% larger. The chemical valence of impurities becomes secondary in the presence of these high strains. A potentially unique choice as an alternative dopant could therefore be Ag, which has roughly the same ionic radius as Y and Ca, and can also be isovalent with Y so that it would not have any direct effect on the hole concentration in the grains. These dopants might increase the superconducting current across the grain boundary like Ca, but without detrimental effects on superconducting properties inside the grain.

We conclude that Ca substitution at the grain boundary occurs in order to reduce the local strain. In turn, the concomitant strain relief has a major effect on the O vacancy formation energies in the vicinity. Our calculations show that in bulk YBCO, O vacancies form preferentially along the CuO chains, with a formation energy of ~1.9 eV (Fig. 1b); the O vacancy formation energy in the CuO_2 planes is ~0.7 eV higher. Moreover, Fig. 1b shows that in strained, undoped YBCO, the formation energies for O vacancies are significantly reduced, both in the CuO_2 planes and CuO chains. O vacancies would therefore segregate to an undoped grain boundary, explaining the oxygen deficiency and hole depletion known from previous studies[20,21]. When Ca doping is introduced, O vacancy formation energies increase, becoming even higher than in the bulk in the case of the CuO chains. Hence, compared to the undoped grain boundary, the doped grain boundary should show much reduced deficiency of O, and therefore reduced hole depletion. Thus, our results confirm the fact that excess O vacancies in grain boundaries and their corollary effects are the primary reason for the observed reduction in critical currents in poly-crystalline YBCO. The role of Ca doping is to remove the intrinsic excess of O vacancies from YBCO grain boundaries. Thus, high critical currents are restored through a cooperative doping mechanism.

To test the theoretical predictions experimentally, we measured electron energy-loss spectra (EELS) in an aberration-corrected scanning transmission electron microscope (STEM). With a probe size around 1 Å, such instruments are able to provide 'column-by-column' spectroscopy, and directly confirm the effects predicted by theory. Thin films of YBCO, both pristine and 20% Ca doped, were grown by laser ablation on $SrTiO_3$ bicrystal substrates at the University of Göttingen. Superconducting properties were analysed previously, and a 35% increase in J_c was found on Ca doping[13].

The dislocation core structures were found to be quite different in the Ca-doped case as compared to the undoped sample. As shown in Fig. 2, the Ca-doped core shows a complete additional atomic

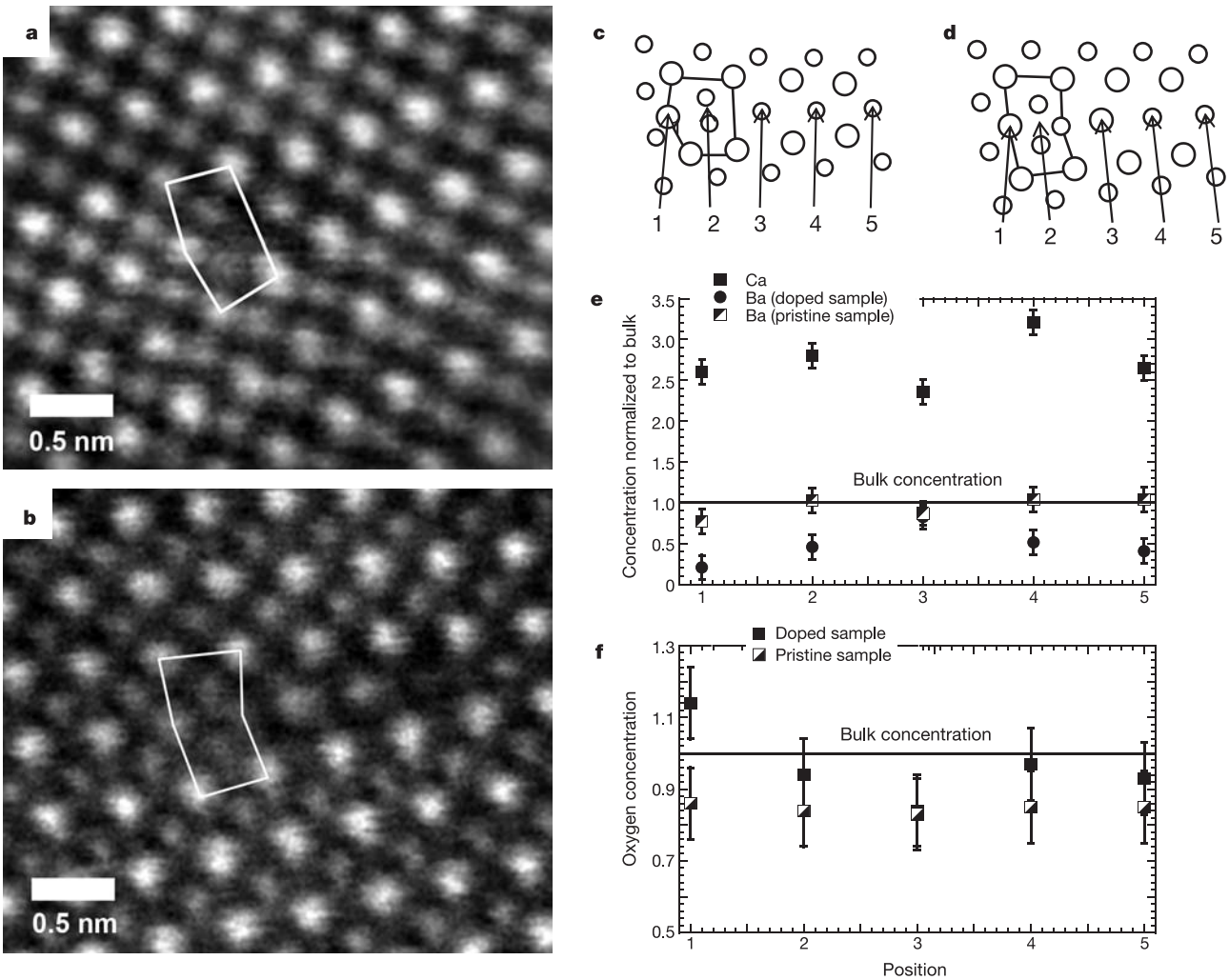

Figure 2 | Structural differences in pristine and Ca-doped YBCO. a, Atomic-resolution *Z*-contrast image of a pristine 4° [001] tilt grain-boundary dislocation core on the Cu-O sublattice, showing the typical pentagonal arrangement[22]. **b**, A Ca-doped grain boundary: the Y/Ba column pentagonal arrangement encloses three columns, two on the Cu-O and one on the Y/Ba sublattice. **c** and **d**, schematic core structure of **a** and **b**, respectively. **e**, Profile of Ca and Ba concentration for probe positions 1–5 indicated in **c** and **d**, normalized to the bulk. **f**, O K-edge quantification for probe positions 1–5, showing less O-deficiency in the doped dislocation cores (error bars indicate the standard error on the concentration quantification).

© 2005 Nature Publishing Group

column at its centre. The column pairs in the undoped dislocation cores are typically seen in perovskite grain boundaries, but in the doped boundary there are instead three columns. These structures were seen consistently over the entire grain boundary. In addition, the lattice perpendicular to the grain boundary is significantly expanded in the Ca-doped sample (from 17% in the pristine core to 53% in the doped core). This expanded region extends for several unit cells, to the right of the core itself. EELS data were taken from the probe positions numbered in the schematic (Fig. 2c and d). The probe size was unchanged from that used for imaging, and therefore provides a column-by-column analysis with the same resolution as the image[22–24]. In the Ca-doped sample, the average increase in Ca concentration was ~2.5 times compared to the bulk, as shown in Fig. 2e. On the right of the core, the columns are nominally Cu–O columns, consistent with the theoretical prediction that Ca should replace Cu in the expanded lattice. At the left of the core, column 1 is nominally a Y/Ba column, and the presence of Ca in this compressed region is again consistent with the theoretical prediction. Furthermore, of the five columns analysed, only column 3 showed a statistically significant decrease in O concentration, as shown in Fig. 2f. All other columns showed an increase in O concentration compared to the undoped dislocation core, which showed 15–20% depletion in O from each of the columns 1–5.

Besides the determination of elemental concentrations, EELS provides a quantitative measure of the carrier concentration from the fine structure on the O K-edge, specifically from the ratio of the pre-peak to the main peak[20,21]. The O pre-peak intensity (see Supplementary Figs S1 and S3) showed substantial reduction in the undoped dislocation core, confirming the expected carrier depletion. In the Ca-doped core (see Supplementary Fig. S2), however, the reduction was much smaller, although still large compared to the bulk value, indicating that significant hole-depletion remains.

The EELS data also explain several consistent changes to the image contrast in the doped core. In all cores observed, column 1, nominally an Y/Ba column, was darker than equivalent columns in the bulk. EELS shows this column to have the highest Ca/Ba ratio, double the bulk value. Because the image contrast is approximately proportional to the square of the atomic number (Z), replacing Ca ($Z = 20$) for Ba ($Z = 56$) would reduce the brightness of the column. On the other hand, column 3, nominally a CuO column, was particularly bright. This column showed the highest Ba concentration (Fig. 2e). Ba is isovalent with Ca, so it is consistent with the principle of maximizing strain relief to replace Ba, with the longest bond to O, in the most highly strained unit cell. Calculations confirmed that Ba substituting for Cu in the chain is also energetically favourable, and again raises the O vacancy formation energy to near its bulk value.

Finally, we compare the present physical model of the role of grain boundaries and Ca doping in YBCO with earlier work. Our model is consistent with the conventional view that grain boundaries in YBCO contain O vacancies, which act as donors and result in positive charge in the grain-boundary plane (the energy bands bend down). The positive charge sets up a space-charge region of hole depletion caused by excess screening electrons. We have shown that, through the cooperative doping mechanism, both the grain-boundary charge and the space-charge region are reduced. These results contrast only with a recent theory paper by Su and Welch[19] and the holography data from Schofield *et al.*[14]. Both these papers concluded that undoped grain boundaries are negatively charged (bands bend up and are completely empty near the grain boundaries, that is, mobile carriers are again depleted) and doping mitigates the effect. We can trace the results of Su and Welch to the fact that they performed calculations for a free surface, and assumed that grain boundaries behave the same way. In addition, these authors only considered Ca substituting for Y. In the case of the holography data, the reported sign of the grain-boundary potential is negative. The discrepancy raises questions about what potential is measured by the holography beam, but these issues are beyond the scope of this Letter. We only note that the question is not settled, as an earlier paper on dislocations in GaN reported a negative potential that could not be accounted for[25].

METHODS

Atomic resolution *Z*-contrast imaging and EELS. We use atomic resolution Z-contrast imaging in the STEM to show the arrangement of the cation columns at the boundary, and correlated EELS to probe the concentration of impurities such as Ca and the local concentration of holes[20–24]. The Z-contrast images were collected using the aberration corrected VG-HB603U with an optimum probe size of 0.6 Å (ref. 26) and a detector inner angle of ~40 mrad. In these collection conditions, the image contrast of an atomic column in the incoherent Z-contrast image is approximately proportional to the square of the average atomic number (Z). This means that the bright spots in Fig. 2 represent the Y/Ba columns, while the less bright columns are Cu-O of the YBCO [001] projection; the O columns are not visible in these micrographs. The additional spot in the Ca-doped dislocation core centre (Fig. 2b) can be directly interpreted as an additional atomic column on the Y/Ba/Ca sublattice, thereby transforming the pentagonal dislocation core in the Ca-doped grain boundary into two bulk-like unit cells under compressive strain.

The correlated energy-loss spectra were acquired using the VG-HB501UX, an aberration-corrected dedicated STEM instrument with a cold-field emission electron gun, operated at 100 kV, and equipped with a Gatan Enfina spectrometer, using an energy dispersion of 0.3 eV per channel, thus yielding a nominal spatial resolution of 1.2 Å and a spectral resolution of 0.4 eV (ref. 24). The spectra were acquired from the bulk and at a specific position in the grain boundary dislocation core structure to measure changes in the Ca L-edge, O K-edge and the Ba M-edge as a function of position in the grain-boundary dislocations. As the excitation energies for the Ca L-edge, the O K-edge and the Ba M-edge are near each other, all three edges can be recorded in a single spectrum. For each position, spectra were acquired for 5 s and several spectra were acquired from similar positions in different dislocation cores to obtain a good signal-to-noise ratio. Sample drift and damage were also checked after each spectrum acquisition. The spectra were then summed and subsequently background-subtracted[27].

Density-functional calculations. Calculations of O vacancy and Ca impurity formation energies were performed using density-functional theory in the local-density approximation[28]. First-principles calculations for realistic, low-angle YBCO grain-boundary structures are computationally prohibitive. As the driving force for defect segregation at the grain boundary is the local strain field, we performed calculations of defect formation energies in biaxially strained YBCO. Ultra-soft pseudopotentials were used to describe electron–ion interactions, and the electronic wavefunctions were expanded in a plane-wave basis set with an energy cut-off of 29 Rydberg. A periodically repeated 52-atom supercell (corresponding to 4 bulk unit cells) was used to minimize defect–defect interactions. All atomic positions were fully relaxed until the quantum-mechanical forces acting on the atoms were negligible.

The formation energies of Ca substitutional impurities were calculated for oxygen-rich conditions, using different amounts of compressive and tensile biaxial lattice strain to mimic the local strain in different regions of the grain boundaries. The formation energy of a Ca impurity substituting for a metal atom A (A = Y, Cu or Ba) in YBCO is given by $\Delta F_{\mathrm{Ca/A}} = -\mu_{\mathrm{Ca}} + \Delta E_{\mathrm{Ca/A}} + \mu_{\mathrm{A}}$, where $\Delta E_{\mathrm{Ca/A}} = E_{\mathrm{Ca}} - E_{\mathrm{A}}$ is the energy required to replace an A atom with a Ca atom in the YBCO supercell, and μ_{Ca} and μ_{A} are the chemical potentials of Ca and A. In oxygen-rich conditions, μ_{A} (and μ_{Ca}) are given by $\mu_{\mathrm{A}} = [E(\mathrm{A}_m\mathrm{O}_n) - n/2\ E(\mathrm{O}_2)]/m$, where $E(\mathrm{A}_m\mathrm{O}_n)$ is the formation energy of the oxide $\mathrm{A}_m\mathrm{O}_n$ (the most stable oxide in the presence of molecular oxygen) and $E(\mathrm{O}_2)$ is the binding energy of the O_2 molecule.

Received 2 December 2004; accepted 14 April 2005.

1. Dimos, D., Chaudhari, P. & Mannhart, J. Superconducting transport properties of grain boundaries in $YBa_2Cu_3O_7$ bicrystals. *Phys. Rev. B* **41**, 4038–4049 (1990).
2. Gross, R. & Mayer, B. Transport processes and noise in $YBa_2Cu_3O_{7-\delta}$ grain-boundary junctions. *Physica C* **180**, 235–242 (1991).
3. Gurevich, A. & Pashitskii, E. A. Current transport through low-angle grain boundaries in high-temperature superconductors. *Phys. Rev. B* **57**, 13878–13893 (1998).
4. Heinig, N. F. *et al.* Evidence for channel conduction in low misorientation angle [001] tilt $YBa_2Cu_3O_{7-x}$ bicrystal films. *Appl. Phys. Lett.* **69**, 577–579 (1996).
5. Hilgenkamp, H. & Mannhart, J. Grain boundaries in high-T_c superconductors. *Rev. Mod. Phys.* **74**, 485–549 (2002).

© 2005 Nature Publishing Group

6. Mannhart, J., Chaudhari, P., Dimos, D., Tsuei, C. C. & McGuire, T. R. Critical currents in [001] grains and across their tilt boundaries in $YBa_2Cu_3O_7$ films. *Phys. Rev. Lett.* **61,** 2476–2479 (1988).
7. Iijima, Y. *et al.* Structural and transport-properties of biaxially aligned $YBa_2Cu_3O_{7-x}$ films on polycrystalline Ni-based alloy with ion-beam-modified buffer layers. *J. Appl. Phys.* **74,** 1905–1911 (1993).
8. Norton, D. P. *et al.* Epitaxial $YBa_2Cu_3O_7$ on biaxially textured nickel (001): An approach to superconducting tapes with high critical current density. *Science* **274,** 755–757 (1996).
9. Hammerl, G. *et al.* Enhanced supercurrent density in polycrystalline $YBa_2Cu_3O_{7-\delta}$ at 77 K from calcium doping of grain boundaries. *Nature* **407,** 162–164 (2000).
10. Schmehl, A. *et al.* Doping-induced enhancement of the critical currents of grain boundaries in $YBa_2Cu_3O_{7-\delta}$. *Europhys. Lett.* **47,** 110–115 (1999).
11. Kucera, J. T. & Bravman, J. C. Transport characterization of calcium-doped $YBa_2Cu_3O_{7-\delta}$ thin films. *Phys. Rev. B* **51,** 8582–8590 (1995).
12. Daniels, G. A., Gurevich, A. & Larbalestier, D. C. Improved strong magnetic field performance of low angle grain boundaries of calcium and oxygen overdoped $YBa_2Cu_3O_x$. *Appl. Phys. Lett.* **77,** 3251–3253 (2000).
13. Guth, K., Krebs, H. U., Freyhardt, H. C. & Jooss, C. Modification of transport properties in low-angle grain boundaries via calcium doping of $YBa_2Cu_3O_{7-\delta}$ thin films. *Phys. Rev. B* **64,** 140508 (2001).
14. Schofield, M. A., Beleggia, M., Zhu, Y. M., Guth, K. & Jooss, C. Direct evidence for negative grain boundary potential in Ca-doped and undoped $YBa_2Cu_3O_{7-x}$. *Phys. Rev. Lett.* **92,** 195502 (2004).
15. Kung, H. *et al.* Dissociation of grain boundary dislocations in $YBa_2Cu_3O_{7-\delta}$-coated conductors. *Phil. Mag. Lett.* **81,** 85–93 (2001).
16. Song, X., Daniels, G. A., Feldmann, D. M., Gurevich, A. & Larbalestier, D. C. Electromagnetic, atomic-structure and chemistry changes induced by Ca-doping of low angle YBCO grain boundaries. *Nature Mater.* (submitted).
17. Kim, M. *et al.* Nonstoichiometry and the electrical activity of grain boundaries in $SrTiO_3$. *Phys. Rev. Lett.* **86,** 4056–4059 (2001).
18. Klie, R. F., Beleggia, M., Zhu, Y., Buban, J. P. & Browning, N. D. Atomic-scale model of the grain boundary potential in perovskite oxides. *Phys. Rev. B* **68,** 214101 (2003).
19. Su, H. B. & Welch, D. O. Effects of space charge, dopants, and strain fields on surfaces and grain boundaries in YBCO compounds. *Supercond. Sci. Technol.* **18,** 24–34 (2005).
20. Browning, N. D. *et al.* The atomic origins of reduced critical currents at [001] tilt grain boundaries in $YBa_2Cu_3O_{7-\delta}$ thin films. *Physica C* **294,** 183–193 (1998).
21. Zhu, Y., Zuo, J. M., Moodenbaugh, A. R. & Suenaga, M. Grain boundary constraint and oxygen deficiency in $YBa_2Cu_3O_7$-δ. *Phil. Mag. A* **70,** 969–984 (1994).
22. Allen, L. J., Findlay, S. D., Lupini, A. R., Oxley, M. P. & Pennycook, S. J. Atomic-resolution electron energy loss spectroscopy imaging in aberration corrected scanning transmission electron microscopy. *Phys. Rev. Lett.* **91,** 105503 (2003).
23. Browning, N. D., Chisholm, M. F. & Pennycook, S. J. Atomic-resolution chemical analysis using a scanning transmission electron microscope. *Nature* **366,** 143–146 (1993).
24. Varela, M. *et al.* Spectroscopic imaging of single atoms within a bulk solid. *Phys. Rev. Lett.* **92,** 095502 (2004).
25. Cherns, D. & Jiao, C. G. Electron holography studies of the charge on dislocations in GaN. *Phys. Rev. Lett.* **87,** 205504 (2001).
26. Nellist, P. D. *et al.* Direct sub-angstrom imaging of a crystal lattice. *Science* **305,** 1741 (2004).
27. Egerton, R. F. *Electron Energy Loss Spectroscopy in the Electron Microscope* (Plenum, New York, 1986).
28. Kresse, G. & Furthmuller, J. Efficient iterative schemes for ab initio total-energy calculations using a plane-wave basis set. *Phys. Rev. B* **54,** 11169–11186 (1996).

Supplementary Information is linked to the online version of the paper at www.nature.com/nature.

Acknowledgements We thank D.W. Gillette for the sample preparation and A.R. Lupini for his help in acquiring the images of Ca-doped YBCO. This work is supported by the US Department of Energy, Division of Materials Sciences, Office of Basic Energy Science and the National Energy Research Scientific Computing Center, supported by the Office of Science of the US Department of Energy.

Author Information Reprints and permissions information is available at npg.nature.com/reprintsandpermissions. The authors declare no competing financial interests. Correspondence and requests for materials should be addressed to R.F.K. (klie@bnl.gov).

© 2005 Nature Publishing Group